Photochemistry and Photobiology, 20**, **: *–*

Characterization of a Smartphone Camera's Response to Ultraviolet A Radiation

Damien Igoe*, Alfio Parisi and Brad Carter

Faculty of Sciences, University of Southern Queensland, Toowoomba, Australia

Received 14 June 2012, accepted 28 July 2012, DOI: 10.1111/j.1751-1097.2012.01216.x

ABSTRACT

As part of a wider study into the use of smartphones as solar ultraviolet radiation monitors, this article characterizes the ultraviolet A (UVA; 320–400 nm) response of a consumer complementary metal oxide semiconductor (CMOS)-based smartphone image sensor in a controlled laboratory environment. The CMOS image sensor in the camera possesses inherent sensitivity to UVA, and despite the attenuation due to the lens and neutral density and wavelength-specific bandpass filters, the measured relative UVA irradiances relative to the incident irradiances range from 0.0065% at 380 nm to 0.0051% at 340 nm. In addition, the sensor demonstrates a predictable response to low-intensity discrete UVA stimuli that can be modelled using the ratio of recorded digital values to the incident UVA irradiance for a given automatic exposure time, and resulting in measurement errors that are typically less than 5%. Our results support the idea that smartphones can be used for scientific monitoring of UVA radiation.

INTRODUCTION

UVA (320–400 nm) accounts for 90–95% of incident solar UV radiation and has considerably more intense irradiance than ultraviolet B (UVB; 1,2). As UVA possesses longer wavelengths than UVB (280–320 nm), they pose a potentially significant biological risk by penetrating further into human skin (3,4). Recent studies strongly suggest a significant link between UVA exposure and skin carcinogenesis and photoaging, thus these wavelengths cannot be ignored in the consideration of skin cancer risk (1,3). The concern is exacerbated by UVA penetration through windows and clothing (4,5). Personal monitoring of UVA exposures is paramount to improve the understanding of the factors influencing the UVA environment. Smartphones are a rapidly proliferating technology of considerable versatility, but are currently underutilized in regard to solar UV monitoring. The Australian Bureau of Meteorology (6) provide iPhone and Android phone apps that allow the user to obtain the UV index (UVI). However, like the UVI forecast in the media, this does not take into account the local cloud and environmental conditions. *Sundroid* is an example of a smartphone app, which with the aid of external UVA and UVB photodiodes, process data to gauge an individual's UV exposure (7). However, this app still requires the use of external sensors, and has not utilized the technology of the phone's built-in camera for sensing of UVA irradiances.

Smartphone cameras predominately use complementary metal oxide semiconductor (CMOS) image sensors (8,9). CMOS image sensors possess an inherent sensitivity to UV wavelengths as small as 200 nm (10). Other important advantages for the use of CMOS in smartphones include low cost, high speed and on-chip functionality (8,11). CMOS image sensor technology has undergone significant improvements in recent years that have significantly enhanced sensitivity to blue and UV wavelengths (12,13). Backside illumination and back-thinned sensors have allowed further UV sensitivity and improvements in quantum efficiency (8,14). Future developments anticipated include the addition of a white pixel to enhance low-light sensitivity, and microlenses that mimic insect eyes (8,15).

Smartphones are an example of the proliferation of customizable consumer electronics and are one of the technological platforms for concepts such as "Participatory Urbanism" and "Citizen Science," where the phone is recast as a personal scientific measurement tool (16). Smartphones have already been used in several other scientific applications. Breslauer *et al.* (17) were able to image blood cells using a mobile phone camera with a modified attachment and task-specific programming. Researchers have also attached gas sensors to smartphones to detect the presence of CO and NO_2 in urban environments (16,18). Smartphone use is increasing, particularly with the younger generations, thus providing an unprecedented opportunity for greater community participation in a broader scientific understanding (8,19). To date, there has been scant research to investigate the potential of the capabilities of a smartphone camera to provide information on the solar UVA.

This article presents the results of research to determine the feasibility and extent to which a smartphone camera, as an example of an accessible off the shelf and versatile mobile technology, can be used as a scientific instrument to measure solar UVA irradiances. Before being tested in the field, the camera's UVA response nevertheless has to be characterized in a controlled environment, so the current study focuses on the required laboratory-based testing.

MATERIALS AND METHODS

*Smartphone selection.*Following investigation of HTC, Huawei and Samsung smartphones, the smartphone selected for testing was the Samsung Galaxy 5 (Samsung Electronics, Seoul, South Korea), on the basis of its useability, cost, and the accessibility of the camera's image data. The Samsung Galaxy 5 phone is lightweight, inexpensive and mass-produced, and the inbuilt camera provides key exposure information such as expo-

*Corresponding author email: damienpaul@gmail.com (Damien Igoe)

sure time (often missing from other brands) essential to relate pixel values to the incident irradiances. The phone camera settings were left at their standard "off the shelf" default values, resulting in pictures saved in JPEG format, and subjected to auto exposure and auto white balance. This approach is to be preferred as obtaining the raw images from any smartphone is both technically very difficult and unnecessary. Use of raw images would unnecessarily complicate the procedure, especially as the compression can be factored into the data analysis, and any camera modification involved risks voiding the camera warranty. The smartphone has a 1 cm diameter outer lens and a 1 mm diameter inner lens. This latter lens is a fixed feature, thus is considered in this research to be part of the image sensor as it is impractical to remove the lens for everyday use.

Lens fluorescence. Fluorescence tests were undertaken to ensure that the response of the camera sensor is due to the incident wavelengths transmitted through the narrow band filter and not due to any fluorescence of the outer smartphone camera lens material. The excised outer lens will be referred to as the lens in this article. The lens was subjected to a range of narrow band irradiances from 340 to 380 nm produced by an irradiation monochromator. The irradiation monochromator comprises a 1600 W xenon arc ozone free lamp (model 66390; Oriel Instruments, Irvine, CA) and a double grating monochromator (model 74125; Oriel Instruments), with a digital exposure controller (model 68591; Oriel Instruments). The monochromator input and output slits were set to 4.5 and 4.0 mm, respectively, and the room maintained at 20°C. Spectral irradiances with and without the excised outer lens were measured with a spectroradiometer for wavelengths in 1 nm increments from 320 to 500 nm. The double grating monochromator spectroradiometer (model DMc150; Bentham Instruments Ltd., Reading, UK) is calibrated to a UV standard lamp with calibration traceable to the NPL (National Physical Laboratory, Teddington, Middlesex, UK). The input optics were provided by a 10 mm diameter diffuser (model D7; Bentham Instruments) connected by a 5 m long, 4 mm diameter optical fiber to the input slit of the monochromator of the spectroradiometer. The output beam of the irradiation monochromator covered the entire diffuser surface.

The spectroradiometer recorded 0.043 ± 0.009 mW m^{-2} nm^{-1} from 400 to 500 nm compared to peaks of 171.2 and 10.9 mW m^{-2} nm^{-1} for the 380 and 340 nm irradiating wavelengths respectively. Thus, no lens fluorescence was observed.

Lens and filter transmittance. A major factor that affects smartphone camera UVA detection is the attenuation of irradiances due to the inner and outer lenses, which is common for all mass-market cameras (8). It was not practical to test the attenuation due to the pixel filters without damaging the image sensor. In addition, as bandpass filters (380 and 340 nm; CVI Melles Griot) to provide responses at two discrete UVA irradiances; and a 1% neutral density (ND1%) filter (XND0001; Asahi Spectra) to prevent pixel saturation were used, further attenuation was measured from the incident irradiance from the monochromator. UVA transmission through the lens and external filters were determined by establishing baseline irradiances, using the spectroradiometer at 20°C, measured at 0.1 nm intervals, 10 nm above and below the discrete target UVA wavelengths from 340 to 390 nm in 10 nm increments from the irradiation monochromator. The transmission of each of the smartphone camera lens, ND1%, 340 and 380 nm bandpass filters and combinations of the lens and each bandpass filter with the ND1% were determined by comparing their attenuated irradiances to the baseline.

The UVA irradiances from the irradiation monochromator in 10 nm increments are shown without the excised outer lens and transmitted through the lens in Fig. 1. Comparison between the irradiation monochromator and the lens attenuated irradiances in Fig. 1 show a pronounced decrease from *ca* 380 to 350 nm, a clearer representation of the lens transmission is in Fig. 2. There is a very clear decrease toward shorter wavelengths in percentage transmission at each of the UVA wavelengths. This drops from 18.9% at 390 nm to 1.1% at 340 nm. Despite the fact that there is a low lens throughput at 340 nm, there is still a measurable amount of transmitted radiation at this wavelength that reaches the sensor.

In combination with bandpass and neutral density filters, the UVA irradiances to the camera sensor are attenuated further. The bandpass filters have considerably different transmissions, with the 340 nm filter having just over 10 times the transmission of that at 380 nm, owing to the age of the respective bandpass filters. Transmission of the neutral density filter was very similar at both 380 and 340 nm. As the lens transmission for 380 nm is *ca* 10 times less than that for 340 nm, the overall transmissions through to the sensor are approximately equal to one another (Table 1). The total transmission of the smartphone camera lens and external filters is of the order of that required to allow measurement of the solar UVA irradiances without saturation of the pixel values.

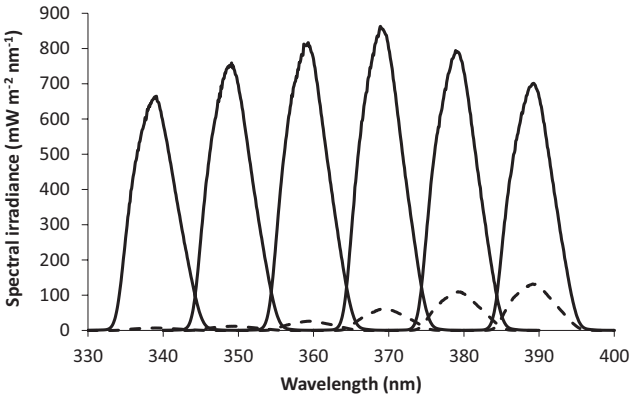

Figure 1. Comparison of the spectral irradiance from the irradiation monochromator (solid lines) to the attenuated irradiance through the excised outer lens (dashed lines).

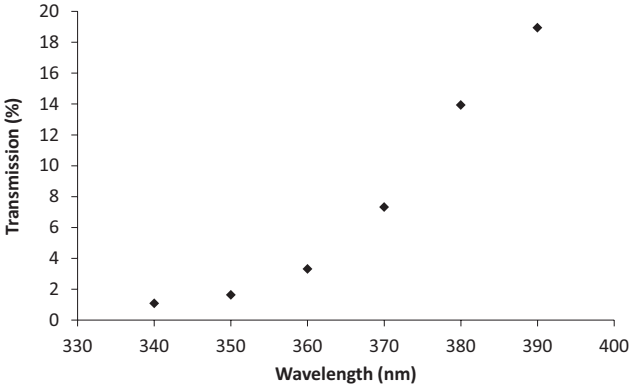

Figure 2. Percentage transmission through the smartphone camera excised outer lens.

Camera response. The camera images recorded contained 8 bit red, green and blue (*RGB*) data, corresponding to absorption depths in the CMOS sensor. The irradiation incident on the camera's image sensor passes through, thus attenuated by the camera's lens, narrow band pass filter and neutral density filter. The irradiation is then converted into an electric current that is in turn converted into digital values out of 255. Obtaining sufficient and relevant red–green–blue digital values will allow an approximation of the sensor irradiance (I_λ) to be calculated using Debevec and Malik's (20) algorithm, linking digital values (Z) and the camera's exposure time (Δt):

$$f(z) = \ln I_\lambda + \ln \Delta t \tag{1}$$

Debevec and Malik (20) state that the luminaire irradiance, in this case from the irradiation monochromator attenuated by the neutral density and bandpass filters, can be used as I_λ. The exposure time (Δt) is automatic in the mobile phone and cannot be practically manipulated. This was retrieved from the photo's digital exchangeable image file data; the *RGB* digital values (Z) from the image sensor, including the lens, were retrieved from the photo's pixel data using the freeware program SciLab (21). The pixel values with the five highest values in each of R, G and B were extracted from each image from three trials and the average for each used in the analysis below. The camera response function (f) was determined by graphing digital values (Z) against the natural logarithm of the product of irradiance and exposure time ($\ln I_\lambda + \ln \Delta t$), incorporating the linear and nonlinear image processes (20). Distances from the mono-

chromator output slit were varied from 10 to 25 cm at 2.5 cm intervals, with the monochromator set at each of the discrete wavelengths of 320, 340, 360 and 380 nm, to provide a range of irradiances, wavelengths and corresponding *RGB* images that were used to characterize the Samsung Galaxy 5 according to Eq. (1).

As the image sensor uses internal filters to discriminate between *RGB*, digital values (*Z*) were calculated as the *RGB* chromatic ratios (*rgb*), calculated by (22):

$$r = \frac{R}{R+G+B} \tag{2}$$

$$g = \frac{G}{R+G+B} \tag{3}$$

$$b = \frac{B}{R+G+B} \tag{4}$$

RESULTS AND DISCUSSION

The bandwidth of incident irradiation from the monochromator as shown in Fig. 1 has a full width at half maximum (FWHM) of *ca* 8 nm.

Camera response

Earlier tests revealed that irradiances greater than *ca* 30 mW m^{-2} resulted in saturation occurring in all three color channels in the smartphone image sensor. It was observed that the red and blue channels saturated first, at *ca* 25 mW m^{-2}, whereas the green channel still yielded measurable signals. The green channel also exhibited the least variation in each trial, as did the chromatic green ratio (Eq. 3).

Green digital values that had very low digital values at less than 10 or at the highest value, 255 were omitted as they represent, respectively, where the signal could not be determined from sensor noise or were saturated. The chromatic g-ratio was compared to the incident irradiation, attenuated by the external filters and camera lens at 340, 360 and 380 nm in Fig. 3. Each plotted point is the average of 15 pixel values for each set of data (five adjoining pixels each from three trials), where the error bars shown represent the standard error. The data for 320 nm were not included as the irradiances through to the sensor were so low as to be within the noise levels. These data were collected in a controlled environment in the absence of visible light. For follow-up research in the field, narrow band filters will be placed over the phone lens with a light tight seal to prevent visible light from reaching the sensor.

The trend from Fig. 3 is two-fold:

1 Irradiances less than *ca* 10 mW m^{-2} result in lower values for the chromatic green ratio, indicating an uneven distribution across the three color channels, as if *RGB* digital values are even, according to Eq. (3), the green chromatic ratio would be close to 0.333. Blue channel digital values are typically considerably higher than the green and red digital channels, as it is exposed to higher energy photons absorbed in the top layers of the image sensor.
2 Irradiances *ca* 10 mW m^{-2} and higher are close to or higher than where all three color channels are equal in value (g = 0.33).

The data were modelled using the base algorithm in Eq. (1) and the chromatic green ratio in Eq. (2) (Fig. 4). Several functions (*f*) were modelled and the best model was found to be as follows:

$$26.4550g^{2.5} - 7.9206 = \ln I_\lambda + \ln \Delta t \tag{5}$$

This model had the strongest correlation coefficient of 0.82 and provides the camera response of the pixel values to the incident UVA irradiance.

Vertical error bars for each data point were calculated using the relevant combination of the standard error of the 15 green pixel values and the standard error of each of the set of 15 pixel values for the *RGB* channels.

Table 1. Percentage transmissions of each and combinations of the elements used in the study. The total transmissions for 360 nm are shown for comparison.

	Transmission (%)		
	340 nm	360 nm	380 nm
Bandpass	35.1	29.2	3.41
ND1%	1.3	1.3	1.4
Bandpass + ND1%	0.46	0.38	0.048
Bandpass + ND1% + lens	0.0051	0.017	0.0065

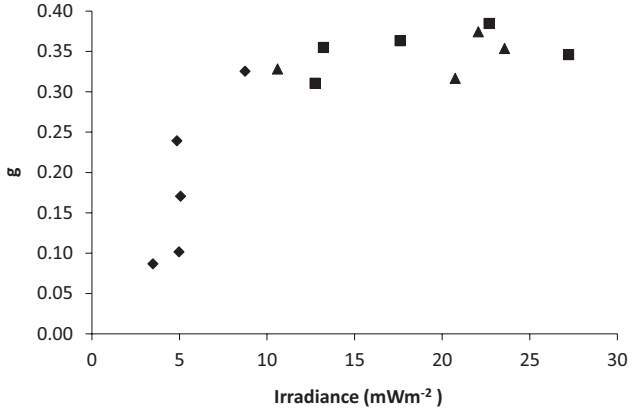

Figure 3. Raw smartphone camera response as a function of irradiance for 340 (squares), 360 (triangles) and 380 nm (diamonds).

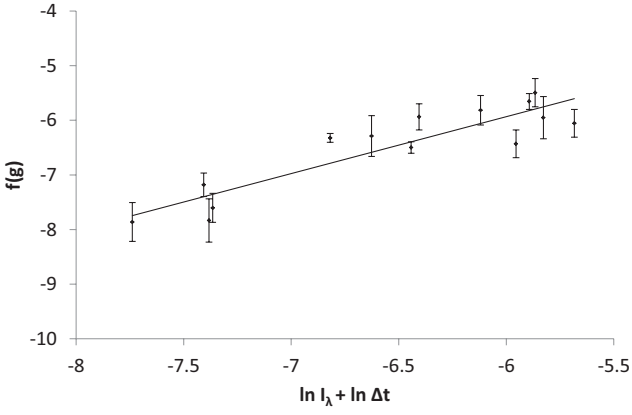

Figure 4. The Samsung Galaxy 5 smartphone camera UVA response.

CONCLUSION

This research has shown that a smartphone image sensor is able to detect useable UVA irradiances. The UVA characterization of a mass-market smartphone camera based on a CMOS image sensor and lens was modelled to produce a relationship between the pixel values and the irradiance. The image sensor operated with its default settings, demonstrated a predictable response to discrete low-intensity UVA irradiance from wavelengths as short as 340 nm. Furthermore, it was established that the camera lens has no fluorescence to UVA wavelengths and provides transmission to wavelengths of 340 nm and higher. These results indicate that with further research the smartphone can become an easy-to-use scientific instrument for UVA radiation-based studies. The availability and accessibility of this device have the potential to greatly increase public and school scientific research interest and participation.

REFERENCES

1. Agar, N., G. Halliday, R. Barnetson, H. Ananthaswamy, M. Wheeler and A. Jones (2004) The basal layer in human squamous tumors harbors more UVA than UVB fingerprint mutations: A role for UVA in human skin carcinogenesis. *PNAS* **101**, 4954–4959.
2. Parisi, A.V., J. Sabburg and M. Kimlin (2004) *Scattered and Filtered Solar UV Measurements*. Kluwer Academic Press, Dordrecht.
3. Zhang, M., A. Queshi, A. Geller, L. Frazier, D. Hunter and J. Han (2012) Use of tanning beds and incidence of skin cancer. *J. Clin. Oncol.* **30**,1588–1593 (In press, DOI: 10.1200/JCO.2011.39.2652)
4. Wang, S., R. Setlow, M. Berwick, D. Polsky, A. Marghoulo, A. Kopf and S. Bart (2001) Ultraviolet A and melanoma: A review. *J. Am. Acad. Dermatol.* **44**, 837–844.
5. Parisi, A.V., D.J. Turnbull and M. Kimlin (2007) Dosimetric and spectzroradiometric investigations of glass filtered solar UV. *Photochem. Photobiol.* **83**, 777–781.
6. Bureau of Meteorology (2012) SunSmart App for iPhone and Android. Available at: http://www.bom.gov.au/uv/iphoneapp.shtml. Accessed on 15 May 2012.
7. Fahrni, T., M. Kuhn, P. Sormmer, R. Wattenhofer and S. Welton (2011) Sundroid: solar radiation awareness with smartphones. UbiComp′11, September 17–21, 2011, Beijing, China.
8. Hayes, T. (2012) Next-generation cell phone cameras. *Opt. Photonics News* **23**, 17–21.
9. Han, C., S. Kwon, S. Lee, E. Kim and K. Sohng (2004) Color correction method for CMOS camera phone images. 2004 IEEE International Symposium on Consumer Electronics, September 1–3, 2004, Reading, United Kingdom 138–141.
10. Tetley, C., Young S. and (2008) Digital infrared and ultraviolet imaging, Part 2: Ultraviolet. *J. Vis. Comm. Med.* **31**(2), 51–60.
11. Luo, B., F. Yang and L. Yan (2010) Key technologies and research development of CMOS image sensors. Second IITA International Conference on Geoscience and Remote Sensing, August 28-31, 2010, Qingdao, China.
12. PhysOrg.com (2011) UV-Transparent Coating for Image Sensors. Available at: http://www.physorg.com/news/2011-02-uv-transparent-coating-image-sensors.html. Accessed on 21 September 2011.
13. Scott, P. (2011) Technology demystified: Backside illuminated sensors. *Cameratechnica*. Available at: http://www.cameratechnica.com/2011/06/23/technology-demystified-backside-illuminated-sensors/. Accessed on 14 April 2012.
14. Jerram, P., D. Burt, V. Hibon, J. Vaillant and Y. Henrion (2010) Back-thinned CMOS sensor optimisation. SPIE Photonics West, San Francisco, January 2010.
15. Rubio, J. (2012) Sony announces new CMOS smartphone camera sensors. IGN, 24 January 2012.
16. Paulos, E., R. Honicky and E. Goodman (2007) Sensing atmosphere. SenSys 2007, 6–9 November, Sydney, Australia.
17. Breslauer, D., R. Maamari, N. Switz, W. Lam and D. Fletcher (2009) Mobile phone based clinical microscopy for global health applications. *PLoS ONE* **4**, 1–6.
18. Westly, E. (2009) Citizen science: How smartphones can aid scientific research. *Pop. Mech.* Available at: http://www.popularmechanics.com/science/4308375. Accessed on 26 January 2012.
19. Palenchar, J. (2010) Smartphone gains brings some pain. *Twice* **25**, 6–.34
20. Debevec, P. and J. Malik (1997) Recovering high dynamic range radiance maps from photographs, pp. 369–376. SIGGRAPH ′97, 3–8 August, Los Angeles.
21. SciLab (2012) Free Open Source Software for Numerical Computation. Available at: http://www.scilab.org/products/scilab/download. Accessed on 15 May 2012.
22. Malacara, D. (2002) *Color Vision and Colorimetry: Theory and Applications*. SPIE Press, Bellingham.